Selective Formic Acid Production via CO_2 Reduction with Visible Light Using a Hybrid of a Perovskite Tantalum Oxynitride and a Binuclear Ruthenium(II) Complex

Fumiaki Yoshitomi,[†] Keita Sekizawa,[†,§] Kazuhiko Maeda,*[,†] and Osamu Ishitani*[,†,‡]
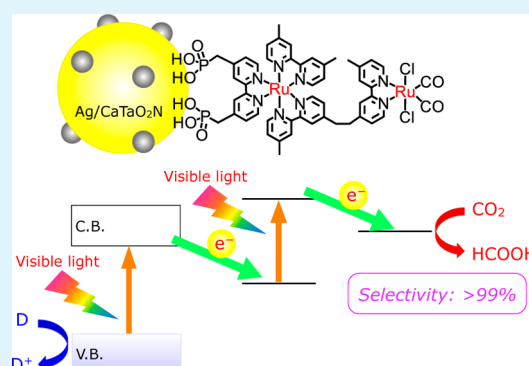
[†]Department of Chemistry, Graduate School of Science and Engineering, Tokyo Institute of Technology, 2-12-1 Ookayama, Meguro-ku, Tokyo 152-8550, Japan

[‡]CREST, Japan Science and Technology Agency, 4-1-8 Honcho, Kawaguchi-shi, Saitama 322-0012, Japan

Ⓢ *Supporting Information*

ABSTRACT: A hybrid material consisting of $CaTaO_2N$ (a perovskite oxynitride semiconductor having a band gap of 2.5 eV) and a binuclear Ru(II) complex photocatalytically produced HCOOH via CO_2 reduction with high selectivity (>99%) under visible light ($\lambda > 400$ nm). Results of photocatalytic reactions, spectroscopic measurements, and electron microscopy observations indicated that the reaction was driven according to a two-step photoexcitation of $CaTaO_2N$ and the Ru photosensitizer unit, where Ag nanoparticles loaded on $CaTaO_2N$ with optimal distribution mediated interfacial electron transfer due to reductive quenching.
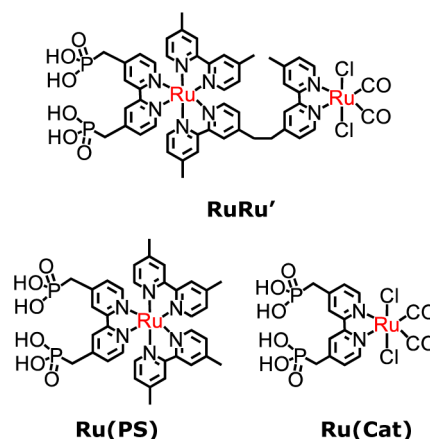
1. INTRODUCTION

Photocatalytic CO_2 reduction into valuable chemicals over a heterogeneous photocatalyst is important in order to establish a reductive half-cycle of artificial photosynthesis.[1−12] In recent years, the production of transportable fuels such as formic acid or methanol has attracted much attention, since these chemicals can act as energy carriers of hydrogen, which outputs a high density of energy after combustion without releasing harmful products.[4−9]

We have been developing CO_2 fixation systems consisting of a semiconductor and a metal complex workable under visible light.[6−9] Among the hybrid systems developed, combining Ag-modified TaON with a binuclear Ru(II) complex (**RuRu′** in Chart 1) allows one to convert CO_2 to HCOOH, according to a two-step photoexcitation mechanism, as depicted in Scheme 1.[6] Under visible light ($\lambda > 400$ nm), both Ag/TaON and the sensitizer unit in **RuRu′** undergo photoexcitation. The conduction band electrons in Ag/TaON migrate to the excited photosensitizer unit, producing a one-electron reduced species (OERS). Subsequently, intramolecular electron transfer takes place from the OERS of the photosensitizer unit to the catalytic unit, because of the downhill nature of the process. Finally, the valence band holes in Ag/TaON oxidize methanol to give formaldehyde, whereas electrons transferred to the catalyst unit reduce CO_2 to formic acid. However, no semiconductor other than TaON has been reported to work as a component of this CO_2 reduction Z-scheme. In addition, the selectivity of

Chart 1. Structures and Abbreviations of Ru Complexes Used in This Work

RuRu′

Ru(PS)   **Ru(Cat)**

HCOOH production remains moderate (~70%), accompanied by appreciable H_2 evolution. Regarding the HCOOH production selectivity, we have been developing another CO_2 reduction photosystem that consists of a Ru(II) complex (e.g.,
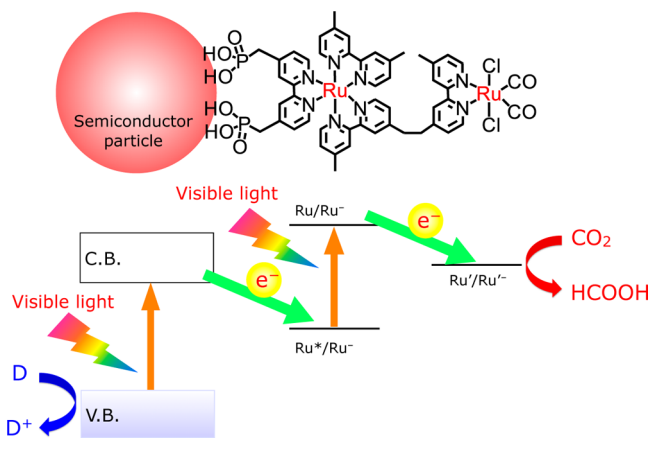
Scheme 1. Z-Scheme CO_2 Reduction under Visible Light Using a Hybrid That Consists of a Semiconductor and a Binuclear Ru Complex

Table 1. Physicochemical Properties of $ATaO_2N$ (A = Ca, Sr, Ba)

semiconductor	band gap[a] (eV)	conduction band potential[b] (V)	specific surface area (m^2 g^{-1})
$CaTaO_2N$	2.5	−2.15	5.6
$SrTaO_2N$	2.1	−1.61	7.1
$BaTaO_2N$	1.8	−1.33	8.9

[a]Estimated from the onset wavelength of diffuse reflectance spectra (see Figure S1B in the Supporting Information). [b]Reported by Balaz et al.[17] and corrected to vs $Ag/AgNO_3$.

Ru(Cat) in Chart 1) and carbon nitride, which respectively work as the catalytic and light-harvesting units.[7−9] In these systems, the selectivity of CO_2 reduction toward HCOOH production remains ∼80%. Therefore, a new semiconductor material that selectively reduces CO_2 into HCOOH under visible light is highly desirable. Selective production of HCOOH (or CO) using $Ru(bpy)(CO)_2(Cl)_2$-type complexes as catalysts in photocatalytic CO_2 reduction is a hot topic, not only in heterogeneous systems but also in homogeneous systems.[13]

As depicted in Scheme 1, it is expected that photocatalytic activity for the Z-scheme CO_2 reduction system will be dependent on the conduction band potential of the semiconductor employed, because it is clear that electron transfer from the semiconductor component to the photosensitizer unit of **RuRu′** plays a key role in the reaction. Here, we employed $ATaO_2N$ (A = Ca, Sr, Ba) perovskites as the component for Z-scheme CO_2 reduction, in combination with the **RuRu′** binuclear complex having a redox photosensitizer and a catalytic unit. $ATaO_2N$ (A = Ca, Sr, Ba) perovskites were originally developed by Domen et al. as visible-light-driven photocatalysts for H_2 evolution from water containing an electron donor.[14−16]

2. RESULTS AND DISCUSSION

$ATaO_2N$ (A = Ca, Sr, Ba) powders were prepared according to the previous literature, with some modifications.[14−16] Details of the structural characterization are included in the Experimental Section. XRD analysis indicated that a single-phase perovskite structure was obtained in all cases (see Figure S1A in the Supporting Information). Based on the onset wavelength of ultraviolet−visible (UV-vis) diffuse reflectance spectra (Figure S1B in the Supporting Information), the band gaps of $ATaO_2N$ (A = Ca, Sr, Ba) were estimated to be ca. 2.5 eV (for Ca), ca. 2.1 eV (for Sr), and ca. 1.8 eV (for Ba). It has also been reported that the conduction band potential (E_{CB}) of $ATaO_2N$ (A = Ca, Sr, Ba) is shifted in the more positive direction from Ca to Ba, because of the relaxation of the distortion in $TaO_{6−x}N_x$ octahedrons, which is accompanied by a decrease in band-gap energy.[14−17] The band-gap energies, which were estimated from the onset wavelength of diffuse reflectance spectra, and the conduction band potentials are listed in Table 1.

First, we tested three perovskite oxynitrides as the semiconductor component of the Z-scheme system, in combination with Ag and **RuRu′**. Among them, it was found that only $CaTaO_2N$ showed reasonable performance. Figure 1 shows
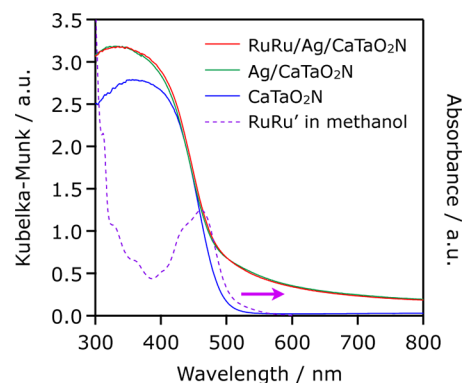
Figure 1. UV-vis diffuse reflectance spectra of $CaTaO_2N$, Ag(1.0 wt %)/$CaTaO_2N$, and **RuRu′** (2.5 μmol g^{-1})/Ag(1.0 wt %)/$CaTaO_2N$. An absorption profile of **RuRu′** in methanol is also shown for comparison, although **RuRu′** was not completely dissolved in methanol. (Hence, we could not determine the molar absorption coefficient.)

UV-vis diffuse reflectance spectra of the $CaTaO_2N$-based hybrid materials, along with an absorption spectrum of **RuRu′** in methanol. Ag-modified $CaTaO_2N$ exhibits a shoulder peak extending to longer wavelengths, which is attributable to the localized surface plasmon resonance of Ag and/or the metallic nature of Ag.[18] Further modification of Ag/$CaTaO_2N$ with **RuRu′** did not alter the absorption profile, because of the overlap of the absorption spectrum of **RuRu′** with that of $CaTaO_2N$. Thus, it is clear that, under visible light (λ > 400 nm), both $CaTaO_2N$ and **RuRu′** undergo photoexcitation. The presence of **RuRu′** on Ag/$CaTaO_2N$ was confirmed by Fourier transform infrared (FT-IR) spectroscopy. As shown in Figure S2 in the Supporting Information, two peaks, which are due to the vibration mode of the two carbonyl ligands in the complex, are observable, even after the adsorption of **RuRu′** on Ag/$CaTaO_2N$.

CO_2 reduction reactions were performed in a DMA(N,N-dimethylacetamide)/TEOA (triethanolamine) (4:1 v/v) mixed solution under CO_2 atmosphere under visible light (λ > 400 nm), and the results are listed in Table 2. Neither $CaTaO_2N$ nor Ag/$CaTaO_2N$ showed activity for the reaction (entries 1 and 2). However, combining Ag/$CaTaO_2N$ with **RuRu′** resulted in clearly observable HCOOH production with high selectivity (>99%) and a turnover number of 32, with respect to the amount of loaded **RuRu′** (entry 3). No H_2 evolution side reaction occurred. Even without Ag loading, the **RuRu′**/

Table 2. Photocatalytic Activities of CaTaO$_2$N with Various Modifications for CO$_2$ Reduction^a

| entry	photocatalyst	solution	atmosphere	Amount of Products (nmol)		
				HCOOH	CO	H$_2$
1	CaTaO$_2$N	DMA/TEOA	CO$_2$	ND	ND	ND
2	Ag/CaTaO$_2$N	DMA/TEOA	CO$_2$	ND	ND	ND
3	**RuRu′**/Ag/CaTaO$_2$N	DMA/TEOA	CO$_2$	320	ND	ND
4	**RuRu′**/CaTaO$_2$N	DMA/TEOA	CO$_2$	93	ND	ND
5	**Ru(Cat)**/Ag/CaTaO$_2$N	DMA/TEOA	CO$_2$	114	ND	2.6
6	**Ru(PS)**/Ag/CaTaO$_2$N	DMA/TEOA	CO$_2$	ND	ND	3.8
7^b	**RuRu′**	DMA/TEOA	CO$_2$	ND	ND	ND
8	**RuRu′**/Ag/CaTaO$_2$N	DMA/TEOA	Ar	ND	ND	ND
9	**RuRu′**/Ag/CaTaO$_2$N	DMA	CO$_2$	ND	ND	ND

^{a}Reaction conditions: photocatalyst, 4.0 mg; solution, a mixture of DMA/TEOA (4:1 v/v) 4 mL; reaction vessel, Pyrex test tube with a septum (8 mL capacity); light source, 400 W xenon lamp with a NaNO$_2$ solution filter. Reaction time: 15 h. In each case, Ru complex of 2.5 μmol g^{-1} was adsorbed. Ag loading amount is 1.0 wt %. ND = not detected. ^{b}In a homogeneous system.

CaTaO$_2$N hybrid could produce HCOOH while maintaining the high selectivity (entry 4), but the activity was much lower than that obtained with Ag. The loading effect of Ag on CaTaO$_2$N will be discussed later in more detail. A control experiment using a model complex of the catalyst unit [represented as **Ru(Cat)**] showed that Ag/CaTaO$_2$N was able to produce HCOOH, accompanied by a tiny amount of H$_2$ (entry 5). In this case, the reaction most likely occurs via direct electron transfer from the conduction band to **Ru(Cat)**. According to our previous investigations, the reduction potential of **Ru(Cat)** is −1.5 V vs Ag/AgNO$_3$,[9] which is more positive than the conduction band potential of CaTaO$_2$N (−2.15 V vs Ag/AgNO$_3$ at pH 7).[17] However, without the catalytic unit but with the photosensitizer unit [**Ru(PS)**] only, no HCOOH production could be identified (entry 6). It is also notable that **RuRu′** dissolved in a DMA/TEOA solution did

not work at all (entry 7). Without CO$_2$ or TEOA, no HCOOH production was observed (entries 8 and 9). No appreciable production of HCOOH was observed in darkness either. These results show that both CaTaO$_2$N and **RuRu′** are essential to realizing HCOOH production, and TEOA works as an electron donor to scavenge holes in the valence band of CaTaO$_2$N.

Ru(II) trisdiimine complexes, including **Ru(PS)**, are known to exhibit emission from the lowest ^{3}MLCT excited state.[19] Figure 2A shows that the emission from **Ru(PS)** on Al$_2$O$_3$, which was monitored at 630 nm, decayed with time. Even in the presence of TEOA, the decay curve remained unchanged, indicating that reductive quenching of the excited state of **Ru(PS)** by TEOA was negligible. By contrast, the emission decay from **Ru(PS)** on CaTaO$_2$N was more pronounced upon addition of TEOA (Figure 2B). In this case, both **Ru(PS)** and CaTaO$_2$N underwent photoexcitation, and the valence band holes in CaTaO$_2$N were scavenged by TEOA. Therefore, the accelerated decay is attributable to the promotion of reductive quenching by electron transfer from the conduction band of CaTaO$_2$N to the excited state of **Ru(PS)**. Note here that oxidative quenching by electron injection from the excited state of **Ru(PS)** ($E_{ox}^* = −1.86$ V)[6] to the conduction band of CaTaO$_2$N ($E_{CB} = −2.15$ V) rarely occurs, because this process is thermodynamically unfavorable.

The photocatalytic performance for the CO$_2$ reduction was dependent on the amount of Ag loaded on the surface of CaTaO$_2$N. As shown in Figure 3, the HCOOH production was enhanced with an increase in the loading amount of Ag to a maximum at 1.0 wt %, then decreased by further deposition. At a loading of 10.0 wt %, no HCOOH was detected. Importantly, neither CO nor H$_2$ was produced in any of the cases, indicating that the selective HCOOH production of this hybrid material was independent of the loading amount of Ag (except for the 10.0 wt % case, which was inactive). The XPS spectrum for Ag 3d of 1.0 wt % Ag/CaTaO$_2$N indicated that the valence state of the loaded Ag is almost entirely metallic (see Figure S3 in the Supporting Information), although the spectral shape is somewhat broad, because of the relatively low concentration of Ag. TEM observations showed that, at the optimal loading, the size of Ag deposited on the CaTaO$_2$N surface ranges from 2 nm to 5 nm, with high dispersion (Figure 4A). However, the inactive material with 10.0 wt % Ag loading consisted of large agglomerates of Ag that covered the CaTaO$_2$N surface excessively (Figure 4B).
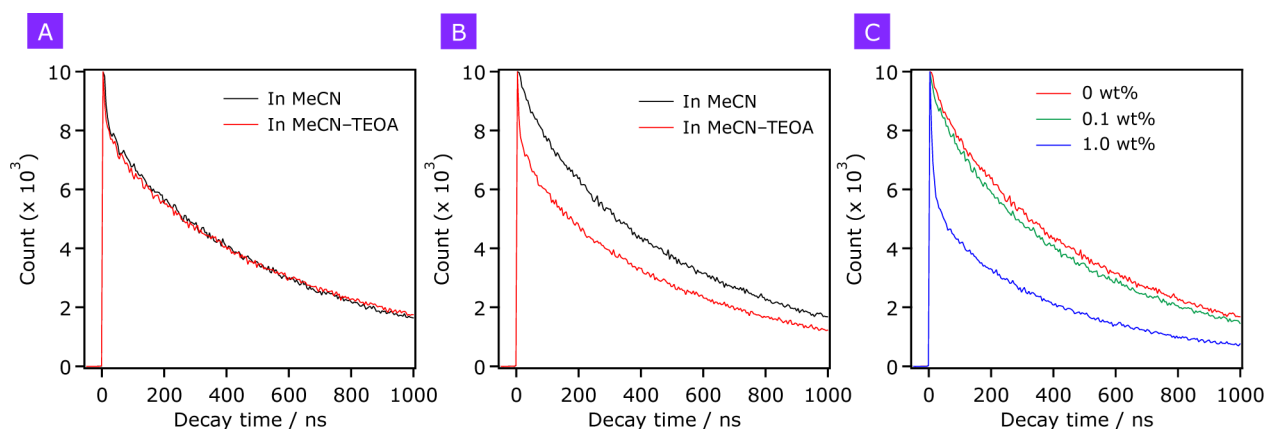

Figure 2. Emission decay profiles of (A) **Ru(PS)**/Al$_2$O$_3$, (B) **Ru(PS)**/CaTaO$_2$N in MeCN with and without TEOA, and (C) **Ru(PS)**/Ag/CaTaO$_2$N with different Ag loadings in MeCN.
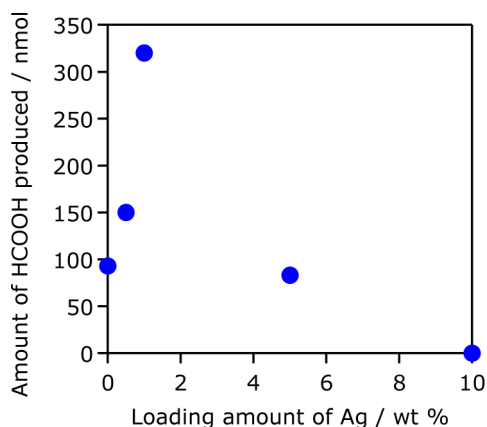
Figure 3. Dependence of photocatalytic activity of **RuRu′**/Ag/CaTaO$_2$N for HCOOH production on the loading amount of Ag. Reaction conditions: photocatalyst, 4.0 mg; solution, a mixture of DMA/TEOA (4:1 v/v) 4 mL; reaction vessel, Pyrex test tube with a septum (8 mL capacity); light source, 400 W xenon lamp with a NaNO$_2$ solution filter. Reaction time: 15 h. **RuRu′** loading: 2.4–2.5 μmol g^{-1}.
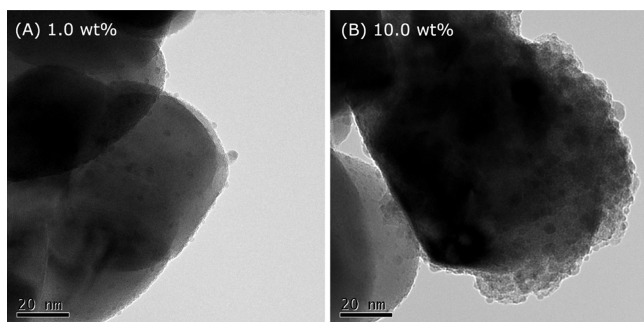
Figure 4. TEM images of CaTaO$_2$N modified with (A) 1.0 wt % Ag and (B) 10.0 wt % Ag.

As we discussed in our previous work,[6] it is considered that the deposited Ag nanoparticles function as electron traps to mediate charge transfer from a semiconductor to the sensitizer unit of **RuRu′** in Z-scheme CO$_2$ reduction. Figure 2C shows emission decay curves of **Ru(PS)** adsorbed on Ag/CaTaO$_2$N under 444 nm photoexcitation. Here, both CaTaO$_2$N and **Ru(PS)** are photoexcited. The emission decay monitored at 630 nm was accelerated upon increasing the loading amount of Ag. As mentioned earlier, oxidative quenching of the excited state of **Ru(PS)** does not occur appreciably. Another control experiment showed that no noticeable change in emission decay from **Ru(PS)** on Al$_2$O$_3$ could be identified even with Ag loading (see Figure S4 in the Supporting Information), indicating that Ag deposits alone did not affect the lifetime of the emission. Therefore, the observed enhancement of emission quenching would be due to the acceleration of reductive quenching of the excited state of **Ru(PS)**, and the loaded Ag plays a role in facilitating the interfacial electron transfer process between Ag/CaTaO$_2$N and **RuRu′**. Kudo et al. reported that Ag nanoparticles act as a co-catalyst for CO$_2$ reduction to CO and HCOOH when they are highly dispersed on BaLa$_4$Ti$_4$O$_{15}$.[3] In the present case, however, Ag deposits on CaTaO$_2$N do not work as a co-catalyst (Table 2, entry 2), but rather as a promoter for interfacial electron transfer. This is the first experimental demonstration of a new functionality of Ag nanoparticles that promotes reductive quenching of **Ru(PS)**,

which is essential in photocatalytic Z-scheme CO$_2$ reduction. However, the exact location of **RuRu′** on Ag/CaTaO$_2$N is not clear at present. Considering the role of Ag (i.e., promoter of interfacial electron transfer) and the fact that the Z-scheme CO$_2$ reduction was promoted by Ag on CaTaO$_2$N, **RuRu′** may exist in close vicinity of the Ag/CaTaO$_2$N interface.

In any photocatalytic CO$_2$ reduction research, it is essential to investigate the origin of the carbon species in the reaction product(s), as surface contaminants (e.g., hydrocarbons and organic acids) may be the source.[20] Therefore, we performed the reduction of ^{13}C-labeled CO$_2$ in a similar manner. After 40 h of visible-light irradiation, the reacted suspension was filtered and the supernatant was analyzed by ^{1}H NMR spectroscopy. As shown in Figure S5 in the Supporting Information, a doublet centered at 8.47 ppm with a coupling constant of $J^{13}_{CH} = 190$ Hz was observed, attributed to the proton bound to the ^{13}C atom in H^{13}COOH. The observed coupling constant is consistent with that reported in our previous work.[7] In addition to the doublet, a singlet peak appeared at 8.47 ppm, which was derived from H^{12}COOH. This singlet was also observed when the reaction was conducted in darkness. Here, the ratio of the integral of the singlet peak area under visible light to that without irradiation was almost unity (1/0.97), indicating that H^{12}COOH detected was produced not photocatalytically but resulted from some contaminants. Furthermore, the ratio of the doublet area to the sum of the doublet and singlet was 78%, meaning that H^{13}COOH was the major product in the reaction. Therefore, we concluded that **RuRu′**/Ag/CaTaO$_2$N is capable of reducing CO$_2$ into HCOOH under visible light.

On the basis of the results of the photocatalytic reactions and time-resolved emission spectroscopy, it is reasonably demonstrated that the hybrid material consisting of Ag/CaTaO$_2$N and **RuRu′** photocatalyzes CO$_2$ reduction to selectively form HCOOH under visible light, according to a two-step photoexcitation mechanism, where CaTaO$_2$N and the sensitizer unit of **RuRu′** are both photoexcited, and Ag nanoparticles mediate electron transfer from CaTaO$_2$N to the sensitizer unit. In contrast to TaON, CaTaO$_2$N became an active semiconductor component for CO$_2$ reduction, even without the sensitizer unit of **RuRu′** (Table 2, entry 5), although some H$_2$ evolution side reaction occurred at the same time. This characteristic behavior might originate from the relatively negative conduction band potential of CaTaO$_2$N, which allows for direct electron transfer to the catalytic Ru complex, similar to our Ru-complex/C$_3$N$_4$ systems for CO$_2$ photoreduction.[7−9] The importance of the conduction band potential was also evidenced by the results of photocatalytic reactions using SrTaO$_2$N and BaTaO$_2$N, where no HCOOH production was detected. In these cases, the back electron transfer from the excited state of the Ru sensitizer unit to the conduction band of SrTaO$_2$N (or BaTaO$_2$N) might occur, because this process is thermodynamically downhill, in contrast to CaTaO$_2$N.

3. CONCLUSIONS

We found that an oxynitride semiconductor of CaTaO$_2$N serves as a building block for Z-scheme CO$_2$ reduction with the aid of a binuclear Ru complex (**RuRu′**) under visible light to produce HCOOH with high selectivity (>99%). The selectivity achieved in this work was the greatest among already reported systems for visible-light-driven CO$_2$ reduction into HCOOH. Physicochemical analyses indicated that modification of CaTaO$_2$N with Ag nanoparticles exhibiting optimal distribution

is essential to facilitate interfacial electron transfer from the conduction band of $CaTaO_2N$ to **RuRu′**.

4. EXPERIMENTAL SECTION

4.1. Synthesis of ATaO₂N (A = Ca, Sr, Ba). Perovskite oxynitrides of $ATaO_2N$ were synthesized by nitriding the corresponding mixed oxides of A and Ta, according to previous reports with some modifications.[14−16,21]

Prior to nitridation, A-Ta mixed oxides were prepared by the polymerized complex method.[22] In cases of Ca−Ta and Sr−Ta mixed oxides, 0.02 mol of $TaCl_5$ (90.0+%; Wako Pure Chemicals) was dissolved in 50 mL of methanol (99.8%; Kanto Chemicals). Next, 0.3 mol of citric acid (CA, 98%; Wako Pure Chemicals) and 0.02 mol of $CaCO_3$ or $SrCO_3$ (99.5%; Kanto Chemicals) were added to the methanol solution with continuous stirring. After the mixture was magnetically stirred for 1 h to afford a transparent solution, 1.2 mol of ethylene glycol (EG, 99.5%; Kanto Chemicals) was added to the solution. In the case of Ba−Ta mixed oxide, 12 mmol of $Ta(OEt)_5$ (99.9%; Wako Pure Chemicals) was dissolved in 100 mL of methanol. Next, 0.12 mol of CA, 12 mmol of $BaCO_3$ (99.5%, Kanto Chemicals), and 0.48 mol of EG were added to the methanol solution with continuous stirring. The obtained clear mixture was gradually heated to ca. 573 K to remove the methanol and accelerate esterification reactions between CA and EG. Upon continuous heating, the solution became a gel, which was a glassy transparent-brown resin. The resin was decomposed in a mantle heater at ca. 673 K, followed by calcination on an Al_2O_3 plate at 873 K for 5 h in ambient air to yield a white powder.

The white precursor powder was subject to nitridation under a flow of NH_3 (100 mL min⁻¹) at 1223 K for 20 h. For the synthesis of $CaTaO_2N$, an excess amount of $CaCO_3$ (Ca/Ta = 1.25) was added into the Ca−Ta precursor to prevent the formation of Ta_3N_5 phase. After nitridation, all samples were washed with water, filtered, and dried at 373 K for 10 h under vacuum.

4.2. Modification of ATaO₂N with Ag Nanoparticles. The as-prepared oxynitrides were modified with Ag nanoparticles via an impregnation method. Two hundred milligrams (200 mg) of $ATaO_2N$ was dispersed in 10 mL of H_2O, followed by the addition of an aqueous $AgNO_3$ (99.8%; Kanto Chemicals) solution (10 mL in total containing a proper amount of $AgNO_3$). After stirring for 2 h at room temperature, the solution was distilled under reduced pressure to remove H_2O. Finally, the resulting solid sample was heated under a flow of H_2 (20 mL min⁻¹) at 473 K for 1 h.

4.3. Adsorption of Ru Complexes on Ag/ATaO₂N. After the as-prepared Ag/ATaO₂N powders (50 mg) were dried by heating at 373 K for 10 h under vacuum, they were dispersed in an acetonitrile solution (25 mL) with dissolved **RuRu′** or **Ru(PS)**. When **Ru(Cat)** was employed, methanol was used as the solvent. The suspension was stirred at room temperature in darkness overnight, to allow for adsorption/desorption equilibrium. The powders obtained were collected by filtration and washed with acetonitrile or methanol (5 mL). These filtrates were collected and concentrated to 25 mL. The amount of adsorbed ruthenium complex was calculated using eq 1:

$$\text{adsorbed amount (mol/g)}$$
$$= \frac{A_{\text{before}} - A_{\text{after}}}{A_{\text{before}}} \times \frac{C(\text{mol/L}) \times (25 \times 10^{-3})(\text{L})}{50 \times 10^{-3}(\text{g})} \quad (1)$$

where A_{before} and A_{after} are the absorbance of the Ru complex employed before and after the adsorption procedure, respectively, and C is the initial concentration of the complex. The as-obtained composite was employed as the photocatalyst for CO_2 reduction.

4.4. Characterization of the As-Prepared Materials. The materials were characterized by X-ray diffraction (XRD) (Model MiniFlex600, Rigaku; Cu Kα radiation), UV-vis diffuse reflectance spectroscopy (DRS) (Model V-565, Jasco), Fourier-transform infrared (FT-IR) spectroscopy (Model FT-IR-610, Jasco), X-ray photoelectron spectroscopy (XPS) (Model ESCA-3400, Shimadzu), and transmission electron microscopy (TEM) (Model JEM-2010F, JEOL). The binding

energies determined by XPS were corrected in reference to the C 1s peak (284.6 eV) for each sample. Brunauer−Emmett−Teller (BET) surface area was measured using a BELSOEP-miniII instrument (BEL Japan) at liquid nitrogen temperature.

4.5. Time-Resolved Emission Measurements. Emission decay profiles were acquired via the single photon counting method, using a FluoroCube spectrometer [Emission Decay; excitation light source: nanoLED-440 (λ_{ex} = 444 nm); detector: Model TBX-04, Horiba (λ_{ob} = 630 nm)]. The spectra were recorded at room temperature using an acetonitrile solution (4.0 mL) containing a solid sample (3.0 mg) adsorbed with **Ru(PS)** (1.0 μmol g⁻¹). The suspension was bubbled with argon gas for 20 min prior to the measurement.

4.6. Photocatalytic Reaction. Reactions were performed at room temperature using an 8 mL test tube that contained 4 mL of solution (20 vol % triethanolamine in DMA) and 4 mg of photocatalyst powder. Prior to irradiation, the suspension was purged with CO_2 (Taiyo Nippon Sanso Co., >99.995%) for 20 min. A 400 W high-pressure Hg lamp (SEN) was employed as a light source, in combination with an aqueous $NaNO_2$ solution to allow for visible light irradiation (λ > 400 nm). The gaseous reaction products were analyzed using a gas chromatograph with a TCD detector (GL Science, Model GC323), an active carbon column, and argon carrier gas. HCOOH generated in the liquid phase was analyzed using a capillary-electrophoresis system (Otsuka Electronics Co., Model CAPI-3300). As a control, a blank experiment was conducted in a similar manner but without irradiation.

4.7. Isotope-Tracer Experiments. $^{13}CO_2$ (^{13}C, 99%) was purchased from Aldrich Co. We checked the contamination of $H^{13}COOH$ in the $^{13}CO_2$ gas by ^1H NMR spectroscopy. The $^{13}CO_2$ gas was introduced into a DMA-d_9−TEOA (4:1 v/v, 1 mL) solution containing 4.0 mg of the photocatalyst powder after degassing them by freeze−pump−thaw cycling. The ^1H NMR spectra of reaction solutions were measured using a JEOL Model JNM-ECA 400 spectrometer. Before measurements, solids were removed by filtration. The residual protons of DMA-d_9 were used as an internal standard for the measurement.

■ ASSOCIATED CONTENT

ⓢ Supporting Information

Additional characterization data and the result of isotope tracer experiments. The Supporting Information is available free of charge on the ACS Publications website at DOI: 10.1021/acsami.5b03509.

■ AUTHOR INFORMATION

Corresponding Authors
*E-mail: maedak@chem.titech.ac.jp (K. Maeda).
*E-mail: ishitani@chem.titech.ac.jp (O. Ishitani).

Present Address
§Toyota Central Research & Development Laboratories, Inc., 41-1 Yokomichi, Nagakute, Aichi 480-1192, Japan.

Notes
The authors declare no competing financial interest.

■ ACKNOWLEDGMENTS

■ REFERENCES

(1) Kohno, Y.; Tanaka, T.; Funabiki, T.; Yoshida, S. Photoreduction of Carbon Dioxide with Methane over ZrO_2. *Chem. Lett.* **1997**, 26, 993−994.

(2) Teramura, K.; Wang, Z.; Hosokawa, S.; Sakata, Y.; Tanaka, T. A Doping Technique Suppressing Undesirable H$_2$ Evolution Derived from Overall Water Splitting in Highly Selective Photocatalytic Conversion of CO$_2$ in and by Water. *Chem.—Eur. J.* **2014**, *20*, 9906−9909.

(3) Iizuka, K.; Wato, T.; Miseki, Y.; Saito, K.; Kudo, A. Photocatalytic Reduction of Carbon Dioxide over Ag Cocatalyst-Loaded ALa$_4$Ti$_4$O$_{15}$ (A = Ca, Sr, and Ba) Using Water as a Reducing Reagent. *J. Am. Chem. Soc.* **2011**, *133*, 20863−20868.

(4) Sato, S.; Morikawa, T.; Saeki, S.; Kajino, T.; Motohiro, T. Visible-Light-Induced Selective CO$_2$ Reduction Utilizing a Ruthenium Complex Electrocatalyst Linked to a *p*-Type Nitrogen-Doped Ta$_2$O$_5$ Semiconductor. *Angew. Chem., Int. Ed.* **2010**, *49*, 5101−5105.

(5) Suzuki, T. M.; Tanaka, H.; Morikawa, T.; Iwaki, M.; Sato, S.; Saeki, S.; Inoue, M.; Kajino, T.; Motohiro, T. Direct Assembly Synthesis of Metal Complex−Semiconductor Hybrid Photocatalysts Anchored by Phosphonate for Highly Efficient CO$_2$ Reduction. *Chem. Commun.* **2011**, *47*, 8673−8675.

(6) Sekizawa, K.; Maeda, K.; Koike, K.; Domen, K.; Ishitani, O. Artificial Z-Scheme Constructed with a Supramolecular Metal Complex and Semiconductor for the Photocatalytic Reduction of CO$_2$. *J. Am. Chem. Soc.* **2013**, *135*, 4596−4599.

(7) Maeda, K.; Sekizawa, K.; Ishitani, O. A Polymeric-Semiconductor−Metal-Complex Hybrid Photocatalyst for Visible-Light CO$_2$ Reduction. *Chem. Commun.* **2013**, *49*, 10127−10129.

(8) Maeda, K.; Kuriki, R.; Zhang, X.; Wang, X.; Ishitani, O. The Effect of the Pore-Wall Structure of Carbon Nitride on Photocatalytic CO$_2$ Reduction under Visible Light. *J. Mater. Chem. A* **2014**, *2*, 15146−15151.

(9) Kuriki, R.; Sekizawa, K.; Ishitani, O.; Maeda, K. Visible-Light-Driven CO$_2$ Reduction with Carbon Nitride: Enhancing the Activity of Ruthenium Catalysts. *Angew. Chem., Int. Ed.* **2015**, *54*, 2406−2409.

(10) Hong, J.; Zhang, W.; Wang, Y.; Zhou, T.; Xu, R. Photocatalytic Reduction of Carbon Dioxide over Self-Assembled Carbon Nitride and Layered Double Hydroxide: The Role of Carbon Dioxide Enrichment. *ChemCatChem* **2014**, *6*, 2315−2321.

(11) Wang, S.; Yao, W.; Lin, J.; Ding, Z.; Wang, X. Cobalt Imidazolate Metal−Organic Frameworks Photosplit CO$_2$ under Mild Reaction Conditions. *Angew. Chem., Int. Ed.* **2014**, *53*, 1034−1038.

(12) Wang, S.; Lin, J.; Wang, X. Semiconductor−Redox Catalysis Promoted by Metal−Organic Frameworks for CO$_2$ Reduction. *Phys. Chem. Chem. Phys.* **2014**, *16*, 14656−14660.

(13) Kuramochi, Y.; Itabashi, J.; Fukaya, K.; Enomoto, A.; Yoshida, M.; Ishida, H. Unexpected Effect of Catalyst Concentration on Photochemical CO$_2$ Reduction by *trans*(Cl)-Ru(bpy)(CO)$_2$Cl$_2$: New Mechanistic Insight into the CO/HCOO$^-$ Selectivity. *Chem. Sci.* **2015**, *6*, 3063−3074.

(14) Yamasita, D.; Takata, T.; Hara, M.; Kondo, J. N.; Domen, K. Recent Progress of Visible-Light-Driven Heterogeneous Photocatalysts for Overall Water Splitting. *Solid State Ionics* **2004**, *172*, 591−595.

(15) Higashi, M.; Abe, R.; Teramura, K.; Takata, T.; Ohtani, B.; Domen, K. Two Step Water Splitting into H$_2$ and O$_2$ under Visible Light by ATaO$_2$N (A = Ca, Sr, Ba) and WO$_3$ with IO$_3^-$/I$^-$ Shuttle Redox Mediator. *Chem. Phys. Lett.* **2008**, *452*, 120−123.

(16) Higashi, M.; Abe, R.; Takata, T.; Domen, K. Photocatalytic Overall Water Splitting under Visible Light Using ATaO$_2$N (A = Ca, Sr, Ba) and WO$_3$ in a IO$_3^-$/I$^-$ Shuttle Redox Mediated System. *Chem. Mater.* **2009**, *21*, 1543−1549.

(17) Balaz, S.; Porter, S. H.; Woodward, P. M.; Brillson, L. J. Electronic Structure of Tantalum Oxynitride Perovskite Photocatalysts. *Chem. Mater.* **2013**, *25*, 3337−3343.

(18) Mori, K.; Kawashima, M.; Che, M.; Yamashita, H. Enhancement of the Photoinduced Oxidation Activity of a Ruthenium(II) Complex Anchored on Silica-Coated Silver Nanoparticles by Localized Surface Plasmon Resonance. *Angew. Chem., Int. Ed.* **2010**, *49*, 8598−8601.

(19) Hashimoto, K.; Hiramoto, M.; Lever, A. B. P.; Sakata, T. Luminescence Decay of Ruthenium(II) Complexes Adsorbed on Metal Oxide Powders *In Vacuo*: Energy Gap Dependence of the Electron-Transfer Rate. *J. Phys. Chem.* **1988**, *92*, 1016−1018.

(20) Yui, T.; Kan, A.; Saitoh, C.; Koike, K.; Ibusuki, T.; Ishitani, O. Photochemical Reduction of CO$_2$ Using TiO$_2$: Effects of Organic Adsorbates on TiO$_2$ and Deposition of Pd onto TiO$_2$. *ACS Appl. Mater. Interfaces* **2011**, *3*, 2594−2600.

(21) Maeda, K.; Domen, K. Preparation of BaZrO$_3$−BaTaO$_2$N Solid Solutions and the Photocatalytic Activities for Water Reduction and Oxidation under Visible Light. *J. Catal.* **2014**, *310*, 67−74.

(22) Kakihana, M. Sol−Gel Preparation of High Temperature Superconducting Oxides. *J. Sol−Gel Sci. Technol.* **1996**, *6*, 7−55.